Surface x-ray-diffraction study and quantum well analysis of the growth and atomic-layer structure of ultrathin Pb/Si(111) films

P. Czoschke,[1,2] Hawoong Hong,[2] L. Basile,[1,2] and T.-C. Chiang[1,2,*]
[1]*Department of Physics, University of Illinois at Urbana-Champaign, 1110 W. Green Street, Urbana, Illinois 61801-3080, USA*
[2]*Frederick Seitz Materials Research Laboratory, University of Illinois at Urbana-Champaign, 104 S. Goodwin Avenue, Urbana, Illinois 61801-2902, USA*
(Received 20 December 2004; published 5 July 2005)

We present surface x-ray-diffraction results from Pb films grown on pretreated Si(111) substrates at 110 K. Time-resolved data show that the films follow a metastable layer-by-layer growth mode. The resulting film roughness is small, allowing for a thickness-dependent study of the film layer structure and its distortion (strain) relative to the bulk. The strain arises as a result of quantum confinement of the electrons in the film, which leads to charge distortions similar to Friedel oscillations. The charge distortions in turn lead to lattice distortions, for which two models are derived based on a free-electron gas confined to a quantum well. Extended x-ray-reflectivity data show evidence of quasibilayer distortions in the film, which are well described by the free-electron models. Oscillations in the relaxations of the Pb layers closest to the film boundaries as a function of thickness are also observed. Calculations of the net expansion or contraction of the films as a function of thickness are made that also exhibit quasibilayer variations and are consistent with the results of previous studies.

DOI: 10.1103/PhysRevB.72.035305 PACS number(s): 73.21.Fg, 61.10.Kw, 68.55.Jk

I. INTRODUCTION

With the smallest feature size on current electronic devices already approaching the atomic scale, a fundamental understanding of the physical consequences of shrinking such devices becomes increasingly important. When the thickness of a metal film or the size of a nanostructure becomes comparable to the quantum coherence length of its electrons, effects due to confinement and quantization of the allowed electronic states are significant in a variety of different physical properties.[1–14] These so-called quantum size effects (QSE) have been the focus of numerous studies and shown to have a significant impact on film growth and morphology.[14–24] One of the effects for which there is less experimental data available is the impact quantum confinement has on the lattice structural distortion (strain) of atomic-scale metal films relative to the bulk. Scanning tunneling microscopy (STM) and helium-atom scattering (HAS) experiments have all reported lattice distortions related to QSE;[25–27] however, these techniques probe primarily the electron density at the surface of the sample, shedding little light on the internal film or buried interface structure. A study using x rays, which scatter primarily off the electrons bound to the atomic cores and have long penetration lengths, can thus provide valuable complementary information to the existing body of work.

We chose to examine Pb films grown on Si(111) using surface x-ray diffraction. Because of the free-electron-like nature of Pb, such films serve as prototypical metal-on-semiconductor systems and have already proved to exhibit strong effects due to QSE, most notably the "preferred thickness" effect, which leads to unusual growth behaviors and the formation of self-assembled islands of uniform height.[16,23,28–31] At the temperature chosen for this study, though, we found that the films follow a layer-by-layer growth mode, which allows us to examine thicknesses that are metastable with respect to the overall energy landscape[24] as well as stable thicknesses. When the structure of these films is studied in detail, quasibilayer distortions are found in the atomic-layer structure of the films consistent with a period of half the Fermi wavelength, which is characteristic of QSE phenomena. We presented a limited study in a previous work that demonstrated the general phenomenon.[22] Here we provide a comprehensive analysis of the data set using two different models that are developed in detail. In addition, different methods are used to analyze the data to test the robustness of the results.

A number of theoretical studies have shown that oscillations in the electron density near the surface of truncated bulk metals can have a significant impact on the atomic-layer structure near the surface.[32,33] The relationship of these boundary effects to QSE in films will be explained and clarified with the aid of model calculations. Although a self-consistent calculation, including such effects as screening and exchange-correlation, similar to the work on metal surfaces, would undoubtedly yield the most accurate description of such lattice relaxations, the aim of this study is to present empirical evidence for such lattice distortions. As such, we develop a simple model based on a free-electron gas that captures the essential features of electron confinement but provides adjustable parameters that can be incorporated into a fitting algorithm used to explain the experimental observations.

II. EXPERIMENT

The experiments were conducted using the surface x-ray-diffraction station at UNICAT (University, National Laboratory, Industry Collaborative Access Team), Sector 33ID, Advanced Photon Source, Argonne National Laboratory.

Diffraction data were obtained using a six-circle goniometer integrated with an ultrahigh vacuum chamber that has a base pressure of 6×10^{-11} torr. X rays at 19.9 keV were obtained from an undulator source using a channel-cut double-Si(111) crystal monochromator with sagittal focusing. Vertical focusing and harmonic rejection was accomplished with a pair of Rh-striped mirrors. The 10×40 mm substrates were cut from P-doped commercial wafers with a nominal resistivity of 1–30 Ω cm. They were thermally anchored to a liquid-nitrogen-cooled manipulator and subjected to prolonged outgassing at 600 °C. The clean Si(111) surface was then obtained by flashing the substrate to 1250 °C for ~13 s, which reliably results in a high-quality (7×7) reconstruction as verified by reflection high-energy electron diffraction and x-ray diffraction. The surface was then pretreated by depositing 4.5 Å Pb on it by thermal evaporation from a Knudsen cell, followed by a 10 min anneal at 415 °C to desorb the excess Pb and to form the Pb/Si(111)-$(\sqrt{3}\times\sqrt{3})R30°$ phase with an initial coverage of ~1.1 Pb monolayer, which is equivalent to $\frac{4}{3}$ monolayer in Si units. This pretreatment has been shown to result in bulklike termination of the Si(111) interface upon which smooth Pb films can be grown at low temperatures.[34–39] In our discussion below, this initial Pb wetting layer is included as part of the total thickness or coverage of a film.

Films were grown *in situ* using molecular beam epitaxy at a rate of 0.53 Å/min. The sample temperature was maintained at 110 K during deposition and for all subsequent measurements, as determined by a thermocouple attached to a sample mounting clip. Time-resolved information on the growth behavior and evolving film morphology was obtained by monitoring the reflectivity of the sample at the out-of-phase condition for Pb(111). In addition, at near-integer coverages, film growth was interrupted and the extended specular x-ray reflectivity rod profile measured to determine the detailed film morphology. The integrated intensity of the reflectivity rod was measured either by doing a series of ω scans ("rocking curves") at different values of perpendicular momentum transfer or by doing a series of "ridge scans" on and parallel to the specular condition along the rod. Both methods allow for effective integration and background subtraction of the specularly reflected intensity and were found to be equivalent for the range of momentum transfer studied.

III. ANALYSIS

A. Specular x-ray reflectivity

The x-ray reflectivity was analyzed using a standard kinematic model, taking into account lattice distortions in the Pb atomic layers.[40–42] Since the specular reflectivity does not include any in-plane components of momentum transfer, the lateral structure of the sample is not probed. The integrated intensity is proportional to the square of the structure factor, which is the coherent sum of the contributions from the substrate and the Pb overlayers

$$I(q_z) \propto \mathcal{C}|F_{\mathrm{Si}}(q_z) + F_{\mathrm{Pb}}(q_z)|^2, \tag{1}$$

where $\mathcal{C}$ contains all of the experimental corrections, such as the polarization factor, the Lorentz factor, etc.,[43] and q_z is the momentum transfer component in the z direction (the surface normal). The substrate contribution is that of a bulk-terminated Si(111) crystal

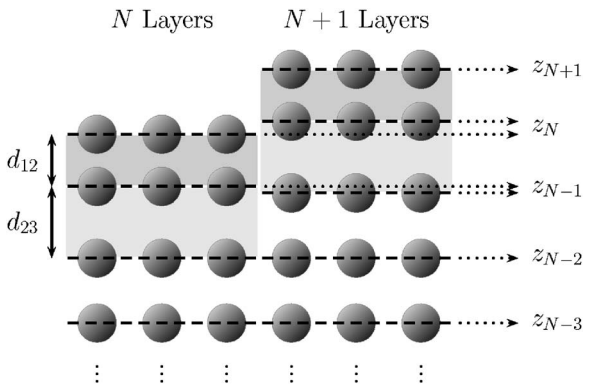

FIG. 1. Roughness in the film will manifest itself at the atomic scale as a distribution of thicknesses $\{N\}$. Since the relaxation of each atomic layer will depend on its position relative to the film boundary, the positions of the layers from regions of different thickness will tend to differ. To account for this effect in the reflectivity, either the exact positions of the layers for each region of thickness need to be known or an effective distribution in z can be used analogous to a Debye-Waller factor.

$$F_{\mathrm{Si}}(q_z) = \left(\frac{a_{\mathrm{Pb}}}{a_{\mathrm{Si}}}\right)^2 f_{\mathrm{Si}}(q_z) e^{-M_{\mathrm{Si}}} \frac{1 + e^{-iq_z a_{\mathrm{Si}}\sqrt{3}/12}}{1 - e^{-iq_z a_{\mathrm{Si}}\sqrt{3}/3}}, \tag{2}$$

where f_{Si} and M_{Si} are the atomic scattering factor and the Debye-Waller factor for Si, respectively, and a_{Si} and a_{Pb} are the lattice constants for Si and Pb. The prefactor of $(a_{\mathrm{Pb}}/a_{\mathrm{Si}})^2$ is included to account for the different atomic surface densities of Si(111) and Pb(111). Using this convention, the Si structure factor is normalized relative to a Pb(111) atomic layer. Following prior work in the literature, the contribution from the Pb overlayers is written as[41,44]

$$F_{\mathrm{Pb}}(q_z) = f_{\mathrm{Pb}}(q_z) \sum_{j=1}^{N_{\max}} \theta_j e^{iq_z z_j} e^{-(1/2)q_z^2 \zeta_j^2}, \tag{3}$$

where $N_{\max}$ is the number of atomic layers in the thickest portion of the film and θ_j is the relative occupancy of layer j. The Debye-Waller-like term accounts for a finite layer distribution in z, where ζ_j is the root-mean-square displacement of the atoms in layer j from their average position z_j, which is measured relative to the Si surface. This term is particularly important in systems with substantial lattice relaxations since the atomic layers in regions of different thicknesses will, in general, not line up. This effect is expected to be larger for near-surface layers, as illustrated in Fig. 1. The ζ_j values for these layers will have a significant component because of the static displacements of the layers in different regions, resulting in a value that depends on j. For films with significant roughness, i.e., with a wide range of thicknesses, the number of independent z_j, θ_j, and ζ_j parameters can become quite large.

Alternatively, in a model that describes the film layer structure more precisely, where the z_j parameters are different for each thickness N, the ζ_j parameters will be approximately independent of j and can be taken outside the sum as a Debye-Waller factor $e^{-M_{\mathrm{Pb}}}$. In such a model, the film contribution to the structure factor is written as

$$F_{\mathrm{Pb}}(q_z) = f_{\mathrm{Pb}}(q_z)e^{-M_{\mathrm{Pb}}}\sum_N p_N \sum_{j=1}^{N} e^{iq_z z_{j,N}}, \tag{4}$$

where p_N is the fractional surface area covered by N Pb layers and the first sum is carried out over all thicknesses present in the film. That is,

$$\theta_j = \sum_{N \geqslant j} p_N, \tag{5}$$

and

$$\sum_N p_N = 1. \tag{6}$$

Generalizing the z_j values to be N dependent will add numerous additional parameters if they are taken as independent degrees of freedom, which can substantially complicate the data analysis. To avoid this difficulty, we derive a physical model based on a confined free-electron gas that describes the lattice distortions. From this model, the $z_{j,N}$ are calculated using only a small number of adjustable parameters, eliminating most of the independent variables. This model for the x-ray reflectivity has far fewer degrees of freedom than the model using Eq. (3), yet was found to reproduce the results with a similar degree of precision, indicating that the $z_{j,N}$ values calculated with the lattice distortion models accurately reflect the actual film morphology.

B. Free-electron model

1. Free-electron charge density

In an attempt to capture the essential physics of an ultrathin metal film, it is reasonable to approximate the system as a free-electron gas that is confined to a one-dimensional infinite quantum well. In this model, the free-electron wave function is subject to the boundary conditions

$$\Psi \to 0 \quad \text{at} \quad z = 0, D,$$

where D is the width of the quantum well. The Fermi sphere of allowed electronic states is correspondingly reduced to a series of subbands, as shown in Fig. 2, each having a wave function

$$\Psi_{\mathbf{k}}(\mathbf{r}) = \sqrt{\frac{2}{V}} e^{ik_x x + ik_y y} \sin(k_z z), \tag{7}$$

where V is the volume of the system and the index k_z can take on the values

$$k_z = \frac{\pi n}{D} \quad n = 1,2,3, \ldots .$$

The electronic charge density at a point $0 \leqslant z \leqslant D$ in the quantum well is then

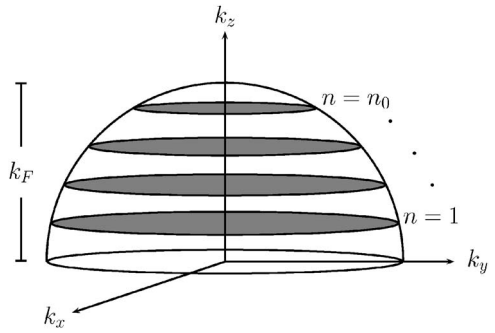

FIG. 2. Because of confinement of the electrons to a quantum well, the Fermi sphere of allowed states is reduced to a set of subbands along the direction of confinement.

$$\begin{aligned}\rho_e(z) &= \frac{2V}{8\pi^3}\int_{|\mathbf{k}|<k_F} (-e)|\Psi_{\mathbf{k}}(z)|^2 d^3\mathbf{k} \\ &= -\frac{e}{\pi D}\sum_{n=1}^{n_0}\left[k_F^2 - \left(\frac{\pi n}{D}\right)^2\right]\sin^2\left(\frac{\pi n z}{D}\right) \\ &= -\frac{e}{2\pi D}\left[C_D - \left(k_F^2 + \frac{1}{4}\frac{\partial^2}{\partial z^2}\right)S_D\left(\frac{2\pi z}{D}\right)\right],\end{aligned} \tag{8}$$

where e is the magnitude of the charge of an electron, k_F is the Fermi wave vector, $n_0 = \mathrm{int}(k_F D/\pi)$ is the quantum number for the highest occupied subband (see Fig. 2), C_D is given by

$$C_D = n_0 k_F^2 - \left(\frac{\pi}{D}\right)^2 \frac{1}{6} n_0(n_0+1)(2n_0+1), \tag{9}$$

and S_D is the dimensionless geometric sum

$$S_D(x) = \sum_{n=1}^{n_0} \cos(nx) = \frac{1}{2}\sin(n_0 x)\cot\left(\frac{x}{2}\right) - \sin^2\left(\frac{n_0 x}{2}\right). \tag{10}$$

The subscripts on $S_D(x)$ and C_D are a reminder that both of these quantities will change with the size of the quantum well. The oscillatory behavior of ρ_e is thus captured in S_D, which gives rise to a n_0-slit interference pattern with a characteristic wavelength of $D/n_0 \approx \pi/k_F = \lambda_F/2$ (one-half of the Fermi wavelength).

We have approximated the film as a quantum well bounded by infinite potential barriers; however, this is clearly only an approximation. The finiteness of these barriers will allow a certain amount of electron density to tunnel into the classically forbidden regions. To account for this effect, we let the well width expand slightly at the film boundaries to allow for a certain amount of charge spillage. In addition, since the film is bounded on one side by the vacuum and the other by the substrate, the amount of spillage at each interface will be different. Thus, we shall define the width of the quantum well to be

$$D = \Delta_s + Nt + \Delta_0, \tag{11}$$

where Δ_s and Δ_0 are the charge spillage distances into the substrate and vacuum, respectively, and t is the average in-

terlayer distance. Given this definition, the coordinate positions of each atomic plane in the absence of any lattice distortions would be

$$z_j = \Delta_s + \left(j - \tfrac{1}{2}\right)t \quad j = 1,2, \ldots, N, \tag{12}$$

where $j=1$ corresponds to the atomic layer closest to the substrate. The introduction of the charge spillage parameters into the model is essentially equivalent to introducing a phase-shift function at the surface, $z=D-\Delta_0$, and another at the buried interface, $z=\Delta_s$.[12] For an infinite barrier, the phase shift has a fixed value of $-\pi$, but by moving the film boundaries by Δ_s and Δ_0, the phase shifts become adjustable and can be made to mimic the actual system. These charge spillage parameters are typically on the order of 0.5 Å. It should be noted that in an actual film the electrons are confined at the substrate interface by the band gap of the silicon, which does not behave exactly like a simple potential barrier. However, as long as the electronic states are confined to the physical extent of the film, the free-electron wave function, Eq. (7), modified with an appropriate phase shift (here simulated with a charge spillage parameter), is a good approximation. In a more detailed model, one might consider the possible energy dependence of the charge spillage parameter. However, the effects of quantum confinement are mainly related to the behavior of the electronic states near the Fermi level. The charge spillage parameter used in this analysis can then be considered to be one appropriate for these states. We have also carried out a separate model calculation based on a finite potential well (at the expense of added complexity), and the resulting form of the total charge density is very similar.

An example of a calculation of the electronic charge density is shown in Fig. 3(a) for a Pb(111) film of seven atomic layers (AL) using physically reasonable parameters. For simplicity, Δ_s and Δ_0 are assumed to be equal for this sample calculation. The electronic charge density exhibits the expected oscillations with a wavelength of $\lambda_F/2$ that dampen away from the two boundaries. This model calculation also illustrates the spillage of the electronic charge beyond the jellium positive background (dotted curve).

As the film thickness decreases, the number of electrons in the film also decreases. At the same time, the separation between the subbands will get larger and there will be a corresponding decrease in the number of states available for the same radius Fermi sphere. Here, we adopt the assumption that the Fermi level may shift slightly so that the electronic charge density deep inside the film is balanced with the positive background from the atomic cores. This charge-neutrality condition minimizes the Coulomb energy of the system and minimizes the electric field within the metal film. We can obtain this condition by extracting the nonoscillatory component of Eq. (8)

$$\overline{\rho_e} = -\frac{e}{2\pi D}\left(C_D + \frac{1}{2}k_F^2\right). \tag{13}$$

Note that this quantity is distinct from the *average* electronic charge density, $\langle \rho_e(z) \rangle$, which is equal to the first term only; the quantity S_D has a zero integral between $z=0$ and D, but

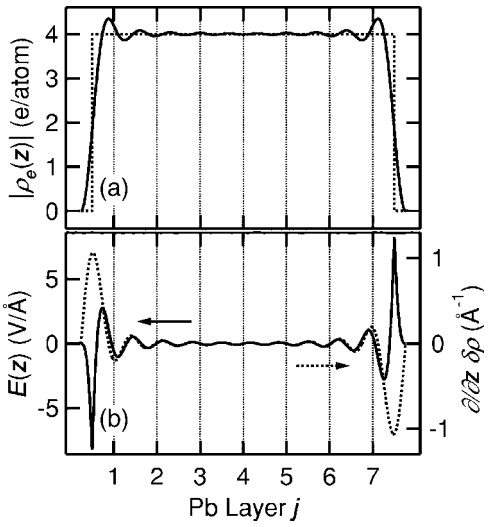

FIG. 3. (a) Electronic charge density (solid curve) with a positive uniform background (dotted lines) for a Pb(111) film with a nominal thickness of 7 AL. The Fermi level is chosen such that the region inside the film is electrically neutral (i.e., the total charge density oscillates about zero). (b) The electric field inside the quantum well (solid curve) compared to the first derivative of the self-normalized charge density variations (dotted curve). Vertical dotted lines indicate the positions of atomic planes in the well where the functions are sampled. The two curves are functionally similar at the atomic planes but differ in the boundary regions.

oscillates about the value $-\frac{1}{2}$ away from the boundaries, as can be seen from Eq. (10). This difference results from the charge spillage tails in $\rho_e(z)$ at the film boundaries, as seen in Fig. 3(a). In the limit $D \to \infty$, the effects of the interfaces become negligible, $C_D \propto D$ and $\overline{\rho_e} \to \langle \rho_e(z) \rangle$. The condition for charge neutrality for any film thickness is given by

$$\overline{\rho_e} = -\frac{N_{\mathrm{val}} e}{A_{\mathrm{cell}} t}$$

or

$$C_D = \frac{2\pi N_{\mathrm{val}} D}{A_{\mathrm{cell}} t} - \frac{1}{2}k_F^2, \tag{14}$$

where N_{val} is the number of itinerant valence electrons per atom of the film material ($N_{\mathrm{val}}=4$ for Pb) and A_{cell} is the area of the surface unit cell. Equation (14) is thus a constraint on k_F, whose solution is shown in Fig. 4. At large film thicknesses, it reduces to the bulk value, as expected. The deviation from the bulk value is smaller than 2% for all integer $N \geqslant 1$.

A different constraint on k_F is obtained if we assume, instead, that the system is an isolated freestanding charge-neutral film, with the total negative electronic charge exactly balanced by the total positive charge of the atomic cores. However, for a film supported on a substrate and in contact with a reservoir of electrons, there can be an interface charge layer and charge conservation must be considered for the entire system, not for the film alone. The requirement of a vanishing electric field within the film represents a better description of our system.

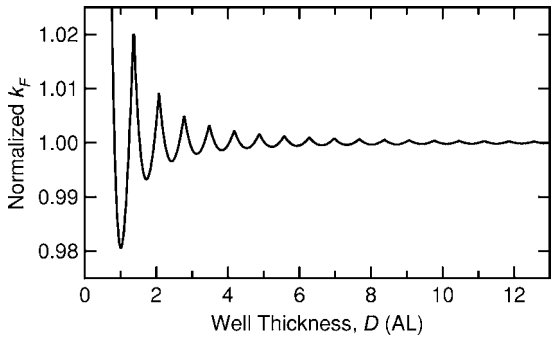

FIG. 4. Fermi wave vector for a Pb(111) film at 110 K as a function of thickness under the condition of charge neutrality inside the film, normalized to the free-electron bulk value.

To relate the lattice distortions to the charge density variations, there are two models that can be followed. Either we can recognize that any lattice distortions due to variations in the charge density will be proportional to the local gradient of the charge density near each atomic plane[22] or we can calculate the electrostatic force on each atomic plane due to the charge distribution of the entire system. Within the local gradient approximation, the positively charged atomic cores move toward regions of higher electronic charge, but the charge distribution away from the point of interest is ignored. The two models actually yield very similar functional forms for the electronic forces, which is to be expected. The electrostatic field corresponds to an integral of the charge density, while the local gradient corresponds to a derivative of the charge density. Since the charge density variations within the film are dominated by sinusoidal oscillations (at a wavelength of $\lambda_F/2$), its integral and derivative should be similar. Numerical results to be presented below confirm that the differences (with proper choices of normalization constants) are small and well within the errors of our analysis. The two models will be developed, in detail, in Secs. III B 2 and III B 3.

2. Local charge density gradient

In this model, we can ignore any uniform positive background (as in the jellium model) because it does not contribute to the derivative anywhere except the two discontinuities at the film boundaries. For simplicity, we consider the self-normalized charge density variations

$$\delta\rho(z) \equiv \frac{\rho_e(z) - \langle\rho_e(z)\rangle}{\langle\rho_e(z)\rangle} = -\frac{1}{C_D}\left(k_F^2 + \frac{1}{4}\frac{\partial^2}{\partial z^2}\right)S_D\left(\frac{2\pi z}{D}\right). \tag{15}$$

Note that in the limit $D\to\infty$, our system changes from a quasi-two-dimensional film into a semi-infinite crystal. In this limit,

$$\lim_{D\to\infty}\delta\rho(z) = -\frac{3}{2}\left(1 + \frac{\partial^2}{\partial u^2}\right)\frac{\sin u}{u} = 3\left(\frac{\cos u}{u^2} - \frac{\sin u}{u^3}\right), \tag{16}$$

where the substitution $u=2k_Fz$ has been made. This equation is the familiar form of the Friedel oscillations in the electron density near the surface of a bulk metal, which we would expect to recover in this limit.

When D is sufficiently large, the charge density variations we have calculated can be well represented by the superposition of the Friedel oscillations associated with the two film boundaries. Intuitively, the Friedel oscillations derived from the two boundaries can overlap and interfere as D becomes small, but the situation is actually more complicated. The Friedel oscillations in a bulk metal arise due to the upper limit to the wave vector (the Fermi level) of electronic states available as Fourier components and the pinning of their relative phases due to the loss of translational symmetry. The states that are available, though, form a continuum from $k=0$ to k_F. In the case of a thin film, the electron wave functions are pinned in phase by both boundaries, giving rise to interference effects. Furthermore, the continuum of k states is reduced to a set of subbands, as shown in Fig. 2. This reduction in the Fourier basis set can also lead to differences from the bulk. In short, charge oscillations in $\rho_e(z)$ and $\delta\rho(z)$ for a film are the result of a phased sum of a discrete set of subband wave functions.

Under the assumption that the displacement of each atomic plane is proportional to the local gradient of the calculated charge density, the change in atomic-layer spacing between layers j and $j+1$ is

$$\Delta t_{j,j+1} = A\left[\frac{\partial}{\partial z}\delta\rho(z_{j+1}) - \frac{\partial}{\partial z}\delta\rho(z_j)\right], \tag{17}$$

where a linear response coefficient A has been included. Since this quantity involves a local difference, the local gradient approximation is expected to work well. In other words, electrostatic fields derived from charges far away from the two atomic layers of interest should have little effect. This method of calculating the lattice distortions results in a model with four adjustable parameters: A, Δ_s, Δ_0, and t. The last quantity should be close but not necessarily identical to the value found in the bulk material.

Note that our numbering convention for the atomic layers differs from that used in many other studies in the literature, where the notation d_{12} is often used to denote the interlayer distance between the two layers closest to the vacuum. Hence,

$$d_{12} = \Delta t_{N-1,N} + t$$

$$d_{23} = \Delta t_{N-2,N-1} + t$$

$$\vdots$$

$$d_{N-1,N} = \Delta t_{1,2} + t.$$

3. Electrostatic force

We need the total charge density to calculate the electrostatic force, including contributions from the positive atomic cores. In keeping with the spirit of the free-electron model, we use a uniform positive (jellium) background,

$$\rho(z) = \rho_e(z) + \frac{N_{\text{val}}e}{A_{\text{cell}}t}[H(z-\Delta_s) - H(z-D+\Delta_0)], \quad (18)$$

where $H(x)$ is the Heaviside step function

$$H(x) = \begin{cases} 0 & x < 0 \\ 1 & x > 0. \end{cases}$$

The electric field is related to the charge density by

$$\frac{\partial}{\partial z}E(z) = \frac{1}{\epsilon_0}\rho(z),$$

where ϵ_0 is the permittivity of the vacuum and E is the z component of the electric field (the only nonzero component, by symmetry). Integrating this equation and using Eqs. (8) and (18) yields

$$\begin{aligned} E(z) &= \frac{1}{\epsilon_0}\int_0^z \rho(z')dz' + E(0) \\ &= -\frac{e}{2\pi\epsilon_0 D}\left[C_D z - \sum_{n=1}^{n_0}\left(\frac{Dk_F^2}{2\pi n} - \frac{\pi n}{2D}\right)\sin\left(\frac{2\pi n z}{D}\right)\right] \\ &\quad + \frac{N_{\text{val}}e}{A_{\text{cell}}t}[R(z-\Delta_s) - R(z-D+\Delta_0)] + E(0) \end{aligned} \quad (19)$$

for the electric field, where $R(x)$ is the ramp function

$$R(x) = \begin{cases} 0 & x < 0 \\ x & x > 0. \end{cases}$$

The atomic cores each have a net charge of $N_{\text{val}}e$ so the change in the interlayer spacing between layers j and $j+1$ is

$$\Delta t_{j,j+1} = \frac{N_{\text{val}}e}{K}[E(z_{j+1}) - E(z_j)], \quad (20)$$

where K is a force constant. Note that the term $E(0)$ from Eq. (19) has no effect on the interlayer spacings.

The electric field model for the lattice distortions also has four adjustable parameters, as with that of Sec. III B 2, with the role of the linear response coefficient A replaced by $1/K$. A comparison of the electric field to the first derivative of the charge density variations is shown in Fig. 3(b). As would be expected, they have a similar functional form over the range where atomic planes are located. The differences can become significant outside the atomic layers because of the tail of charge spillage, but these differences are irrelevant to our analysis of atomic-layer strain.

IV. RESULTS

A. Film growth

During deposition, the growth of the Pb overlayers was monitored by measuring the reflected x-ray intensity at $l=1.65$, where $l=q_z a_{\text{Si}}\sqrt{3}/(2\pi)$ is the perpendicular momentum transfer in Si(111) reciprocal lattice units (1 rlu $=0.668$ Å^{-1}). This point in reciprocal space, halfway between the origin and the Pb(111) Bragg condition, is the lowest-order out-of-phase condition for the Pb overlayers

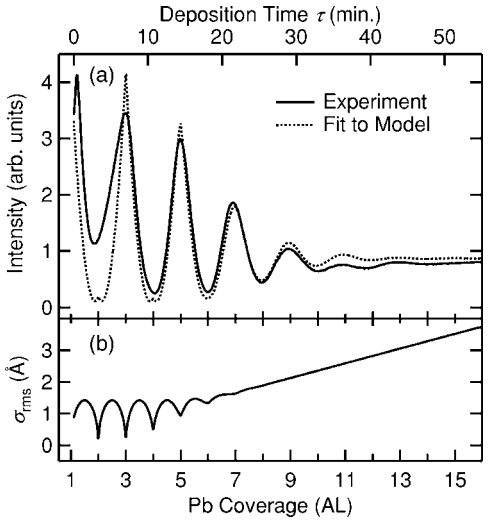

FIG. 5. (a) Experimentally observed oscillations in the reflected x-ray intensity at the out-of-phase point for Pb(111), $l=1.65$, and a fit using the model described in the text. The oscillations every two monolayers indicate that the growth is layer-by-layer, whereas the decay of the oscillations is an indication of increasing roughness, which is shown in (b).

and, as such, is highly sensitive to changes in the surface structure. The initial portion of such a growth curve is shown in Fig. 5. The regular oscillations in the intensity are indicative of layer-by-layer growth,[44] which is independently supported by photoemission measurements.[39] The decay of the oscillations is a result of increasing surface roughness in the film. Quantitative information can be extracted from these data using the model of Sec. III A with a number of simplifying assumptions. First, since we are only measuring one point in reciprocal space, the influence of lattice distortions on the data will be minimal and we may assume the atomic positions of the Pb atoms to be bulklike. Second, to reduce the number of parameters, we assume the distribution of thicknesses $\{p_N\}$ is Gaussian

$$p_N(\tau) = \frac{B(\tau)}{w(\tau)}\exp\left\{-\frac{[N-\Theta(\tau)]^2}{w(\tau)^2}\right\}, \quad (21)$$

where w and Θ are the width of the distribution and the total film coverage [in atomic layers (AL)], respectively, B is a normalization factor selected such that Eq. (6) is satisfied, and τ is the deposition time. Third, we will assume that both w and Θ are linear functions of τ. Note that the parameter w is only obliquely related to the roughness, which is defined as

$$\sigma_{\text{rms}}(\tau) = \frac{t}{\sum_N p_N(\tau)}\sqrt{\sum_N p_N(\tau)[N-\Theta(\tau)]^2}. \quad (22)$$

The results of a fit to this model are shown in Fig. 5(a) as a dotted curve, with the corresponding roughness shown in Fig. 5(b). Considering the simplicity of the model and the number of assumptions it entails, the fit describes the data quite well after about 3 AL. Monitoring of an in-plane su-

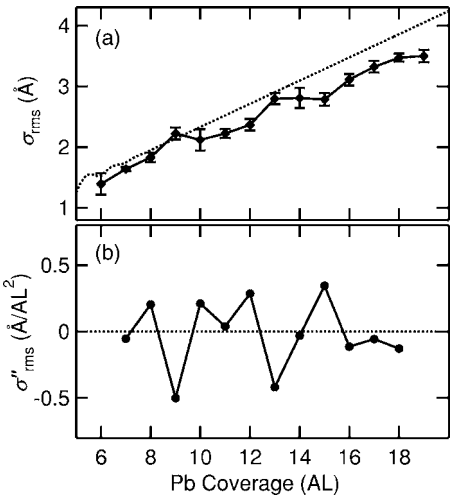

FIG. 6. (a) The deduced roughness of a single film (solid curve) where deposition was interrupted at integer coverages and the extended x-ray reflectivity measured. Error bars are indicative of the range of values obtained using different fitting methods. The dotted curve is the roughness predicted by a fit to the growth curve of the film as in Fig. 5. (b) The discrete second derivative of the data in (a), which shows approximately quasibilayer oscillations in the relative film stability, consistent with oscillations in the surface energy reported in Ref. 24.

perstructure peak from the $(\sqrt{3}\times\sqrt{3})R30°$ interface reconstruction shows it decaying rapidly during the initial phase of deposition. Thus, the behavior of the data for $\Theta<3$ AL is probably affected by the transition of the initially compressed 1.1 monolayer interface layer of the $(\sqrt{3}\times\sqrt{3})R30°$ reconstruction to one of bulklike density.

Using this method, we can determine the initial coverage, rate of deposition, and roughness of the film as a function of time while the film is being grown. With this information, a film of a specific thickness can be obtained by interrupting the deposition at the desired coverage. High-quality films with precise coverages up to 29 AL have been grown using this method. As an additional check, independent measurements of the deposition rate with a quartz-crystal thickness monitor agree with the rates deduced from the fits to the growth curves to within 5%.

A layer-by-layer growth mode with small roughness is important for a study of the thickness dependence of a film's structure. In the case of Pb, this can be problematic because of quasibilayer oscillations in the surface energy,[19,21,23,24] which is the underlying cause of the "preferred-thickness" effect that has been previously reported.[16,23,28–31] In fact, even at 110 K, the growth temperature for this study at which the growth is layer by layer, some influence of the surface energy oscillations can be seen when the film roughness is examined in detail. Figure 6(a) shows the roughness of a film whose growth was interrupted at integer coverages and the extended x-ray reflectivity measured. From fits to the reflectivity (see below), the p_N parameters are determined and a value of the roughness is calculated with Eq. (22). The trend of the roughness values follows closely that predicted from the fit to the deposition curve (dotted curve); however, they do not increase smoothly or even monotonically, with noticeable deviations from the overall trend. This effect is indicative of differences in the relative stability of regions of the film with different thicknesses. For layer-by-layer growth, the distribution of p_N values is peaked about the thickness closest to the coverage, as in Eq. (21), but if that thickness is relatively unstable compared to neighboring thicknesses, the system will tend to be rougher, with the p_N distribution broader than it would be due to normal stochastic effects. Thus, the discrete second derivative of the roughness, σ''_{rms}, is an approximate indicator of the relative stability of the film as a function of thickness. Thicknesses with $\sigma''_{rms}>0$ are relatively stable, whereas thicknesses with $\sigma''_{rms}<0$ are only metastable. These data are shown in Fig. 6(b), and indicate that Pb/Si(111) films of thicknesses $N=8$, 10, 12, and 15 AL are relatively stable and $N=9$ and 13 are only metastable, with σ''_{rms} too close to zero for the other thicknesses to make a prediction. These results are consistent with observations of films grown or annealed at higher temperatures.[16,23,24,28,29] It can therefore be concluded that Pb grown on Si(111) at 110 K follows a metastable layer-by-layer growth mode.

B. Analysis of lattice distortions

Films of integer coverages were grown using the process described above for $\Theta=6-19$ AL. The extended x-ray reflectivity was then measured for each coverage and fit using the methods of Sec. III. Representative examples of the data are shown in Fig. 7, which show some unusual features due to the distorted layer structure of the Pb overlayers. Approximately halfway between the Pb(111), (222), and (333) Bragg peaks at $l\approx3.3$, 6.6, and 9.9 (the last one not shown), respectively, one of the interference fringes is consistently larger than its neighbors. Since they appear near the half-order position for Pb(111), these features are indicative of a bilayer or quasibilayer superperiodicity in the structure of the film. This effect is similar to the superstructure peaks often encountered with surface reconstructions, except in this case the "reconstruction" is in the direction normal to the surface. Since these half-order peaks are much weaker in magnitude than the Pb Bragg peaks, the bilayer distortions are weak and possibly only present in regions near the surface and buried film interface. As can be seen from the dotted curves in Fig. 7, these features cannot be reproduced by a model that does not include lattice distortions in the film layer structure.

The origin of the quasibilayer distortions can be attributed to the variations in the charge density discussed in Sec. III B (see Fig. 3). Such variations are damped oscillations with a characteristic wavelength of $\lambda_F/2$. For bulk Pb(111), this wavelength is 1.98 Å, which is close to $\frac{2}{3}$ the bulk interlayer spacing $t_0=2.84$ Å. Thus, every 2 AL of Pb roughly corresponds to an integer number of oscillations in the charge density. Since the relationship is not exact, the superperiodicity is quasibilayer and the phase of even-odd oscillations can reverse over a sufficiently wide range of thicknesses.

Oscillations are evident in the lattice distortions resulting from the fits to the x-ray reflectivity, an example of which is shown in Fig. 8 for $N=14$. Most of the lattice relaxation occurs in the atomic layers closest to the two film bound-

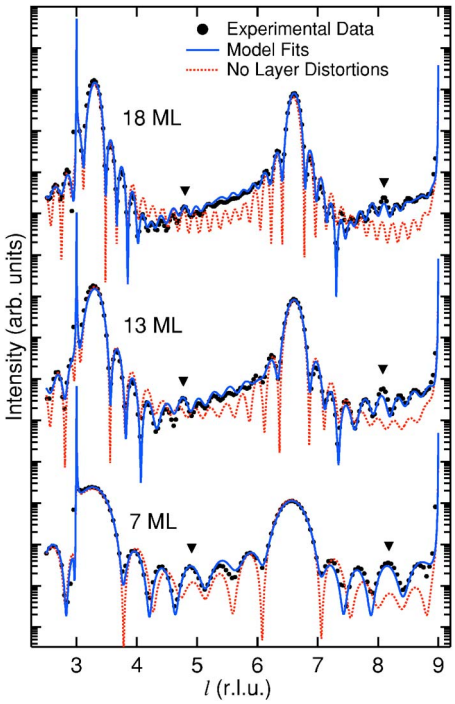

FIG. 7. (Color online) Extended x-ray-reflectivity data (points) for selected coverages. The sharp peaks at $l=3$ and 9 are the Si(111) and (333) Bragg peaks, respectively, while the interference fringes in between are due to the Pb overlayers. The areas marked by inverted triangles are half-order features indicative of a quasibilayer periodicity to the lattice structure of the Pb film. Solid curves are fits using Method B described in the text. Dotted curves are fits with uniform interlayer spacing in the film, which do not represent the data well, especially near the half-order features.

aries, but the quasibilayer distortions penetrate deep into the film as well. An instance of phase reversal (even-odd crossover) is also evident. The overall behavior reflects the force variations as shown in Fig. 3. The asymmetry of the values in Fig. 8 is due to different values for the two charge spillages Δ_s and Δ_0. The results for other thicknesses are qualitatively similar. The thickness dependence of these lattice distortions or relaxations is shown in Fig. 9, where the different sets of data points correspond to four different methods that were used to fit the x-ray data.

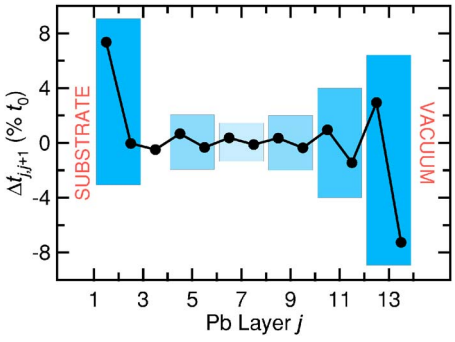

FIG. 8. (Color online) The internal lattice distortions for $N=14$, calculated using Eq. (20) with the parameters from a fit to the extended x-ray reflectivity. Alternations in the distortions are evident, which leads to a quasibilayer superperiod in the lattice structure, as shown with shaded boxes. This effect manifests itself as a weak half-order superstructure peak in the x-ray profiles, as seen in Fig. 7.

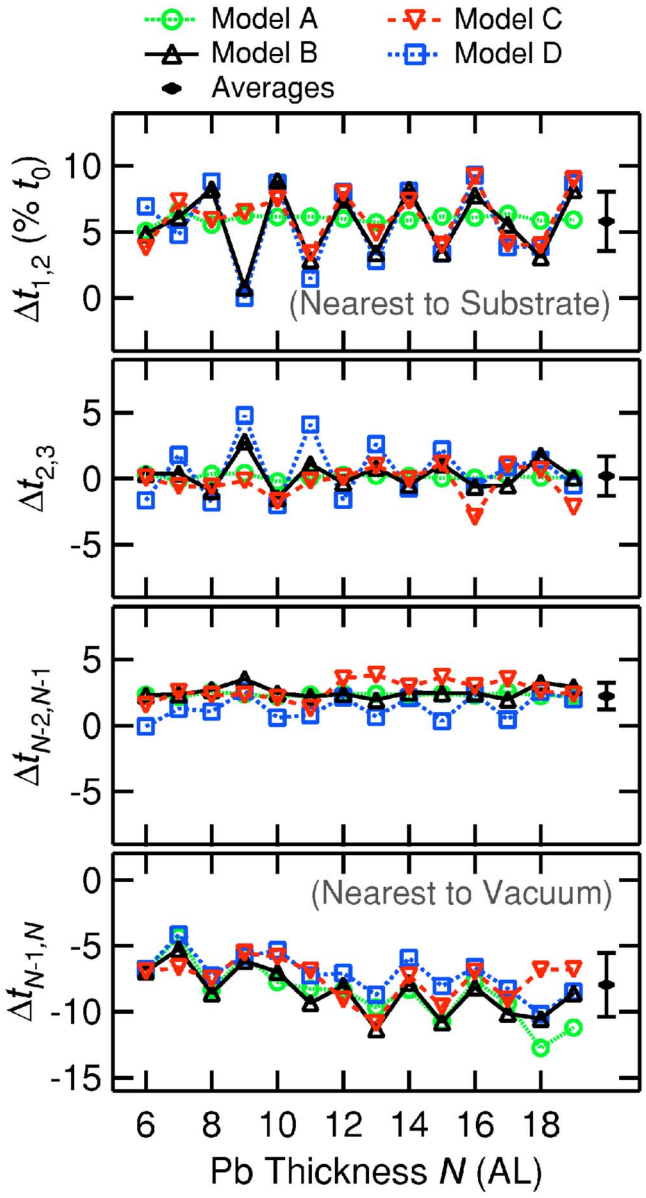

FIG. 9. (Color online) The lattice relaxations for the outer atomic layers for each thickness N, where all values are in percent t_0. The different sets of data points correspond to different fitting methods described in the text. The values for Method A are the values calculated using the parameters for the data set with coverage $\Theta=N$ AL. The points on the far right of each graph represent the values averaged over N for all four methods, along with error bars deduced from the spread in the data.

Method A. The data for each coverage were fit separately using Eq. (4) with the lattice distortions described by Eq. (17), the local charge gradient model. To reduce the number of independent variables, parameters for the lattice distortion model were assumed to be independent of N for any particular coverage, but were allowed to be different for different coverages. This assumption is valid for perfectly smooth

films, but can be inaccurate for rough films. Since these parameters do depend on thickness and the film roughness is not necessarily negligible, the Debye-Waller parameter in Eq. (4) was replaced with ζ_j factors, as in Eq. (3), but only for the Pb layers close to the film boundaries. As a result, this method will be less reliable for extracting the thickness dependence of the lattice distortions, especially for higher coverages since they have the greatest degree of roughness. The results for the two outermost Pb atomic layers at each film interface are shown in Fig. 9 as open circles, where the values for any particular thickness N are taken from the data set whose coverage is N AL (with a distribution of p_N values peaked at that thickness).

Method B. The data for all 14 coverages were fit simultaneously using Eqs. (4) and (17) based on the local charge gradient model for the lattice distortions. With this method, the parameters for the lattice distortion model were N dependent and shared among all the data sets. The other parameters needed to fit the data (the p_N values, Debye-Waller factor, etc.) were separate for each coverage. The results for the lattice relaxations of the outermost layers are shown in Fig. 9 as open upright triangles. Compared to Method A, this method involved fewer fitting parameters since no ζ_j factors were needed.

Method C. As with Method B, all of the data sets for different coverages were fit simultaneously using Eq. (4), but with the lattice distortions calculated using the electrostatic force model, Eq. (20). The same number of parameters were used in the fits as with Method B. The results from this method are shown with open inverted triangles in Fig. 9.

Method D. No model was used for the lattice distortions. Instead it was assumed that any relaxations of the lattice would be limited to the atomic layers closest to the film boundaries. The two interlayer spacings closest to the substrate and the vacuum (four total) were fit as free parameters and were allowed to vary for different N. To keep the number of parameters reasonable, all 14 data sets for different coverages were fit simultaneously as with Methods B and C, sharing the layer expansion parameters. The interlayer spacings for the other Pb layers were assumed to be equal to a separate parameter t, which introduces one additional parameter per data set to the fit compared to Methods B and C. The results from this fit are shown as open squares in Fig. 9.

C. Discussion

All four methods of analysis can be justified on physical grounds as reasonable models to describe the essential features of the system. They involve different constraints on some aspects of the system and, in some cases, very different numbers of fitting parameters, yet they all resulted in fits of comparable quality (measured by χ^2). This is a strong indication that the models reflect the physical system. The spread in the results is an indication of the standard error or level of confidence in the results. The black diamonds and error bars at the right side of the panels in Fig. 9 show that, averaged over the thickness range of study, the top-layer spacing of the Pb film is contracted by $8.0\pm2.4\%$ relative to the bulk, while the next layer spacing is expanded by $2.2\pm1.0\%$. These values are substantially larger than those reported for bulk Pb(111),[45] but are closer to those resulting from recent first-principles calculations for freestanding Pb slabs, which show a contraction of 5–7% in the outermost interlayer spacing and an expansion of 1–3% in the next interlayer spacing.[46] Our results show that the layer spacing closest to the Si substrate is expanded by $5.8\pm2.2\%$, and the next layer spacing is essentially bulklike to within $\pm1.5\%$. In addition to these general trends, which are related to Friedel oscillations associated with the film boundaries, the layer relaxations exhibit quasibilayer oscillations as a function of film thickness that can be attributed to confinement and interference effects. It should be noted that although Methods A, B, and C use models to calculate the z_j parameters, the lattice relaxations reported in Fig. 9 are not theoretically derived values, as in a first-principles calculation, but rather are the empirical results of a direct fit to the experimental data [i.e., the z_j parameters appear explicitly in Eq. (4), the equation used to model the extended x-ray reflectivity]. Therefore, these relaxations should be reasonably model independent. The qualitative agreement of the results using Method D, which fits the experimental data without the use of any model for the lattice distortions, with the results from the other methods is thus a good indication that the lattice relaxations reported are accurate to within the quoted uncertainties.

Representative results of the fits are shown as solid curves in Fig. 7. The fits reproduce the aforementioned half-order features very well, especially compared to the example fits with no lattice distortions, shown as dotted curves. That being said, it was found that other solutions existed with χ^2 values only slightly larger than the best fits. Such solutions primarily differed in the lattice relaxations for $\Delta t_{1,2}$ and $\Delta t_{2,3}$, the two interlayer spacings closest to the substrate. All solutions exhibited strong quasibilayer oscillations; however, they differed in where the crossover from even to odd occurs (i.e., the phase of the oscillations is weakly determined). For example, the turning point that is evident at around $N\approx17$ in the data for $\Delta t_{1,2}$ in Fig. 9 was found at $N\approx13$ and $N\approx11$ in two other solutions with comparable χ^2 values as the best fit. All solutions exhibited similar relaxation values for $\Delta t_{N-1,N}$ and $\Delta t_{N-2,N-1}$, the relaxations of the layers closest to the vacuum. The greater uncertainty in the lattice distortions near the substrate may be due to interfacial roughness from the underlying Si(111) substrate, whose step heights will be incommensurate with the interlayer spacing of the Pb overlayers. However, these errors are no larger than the spread of values determined based on the four different methods of analysis.

In this study, the penetration depth of the x rays used greatly exceeded the thicknesses of all the films studied, thus the interference patterns in the data are due to scattering from all the film overlayers. However, a technique such as STM or HAS, with a short probing depth, will primarily measure the step heights on the surface of the film. To compare with the results of such studies, Fig. 10 shows the deviation of the net film thicknesses from their ideal bulk values and the deduced step heights as functions of N. Each thickness deviation value is the sum of all the lattice distortions (i.e., the $\Delta t_{j,j+1}$ values) for any given N, and the step height values are defined as the difference between two net thicknesses differing

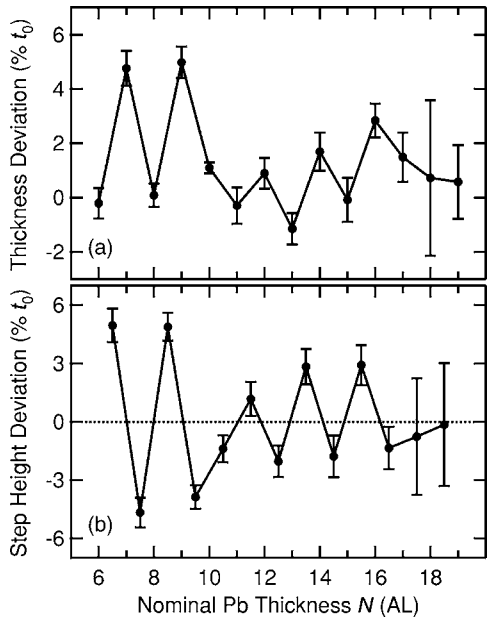

FIG. 10. (a) Net thicknesses calculated from the lattice distortions. Values are the deviation from the ideal thickness Nt_0 in percent t_0. Error bars are representative of the spread in values from the different fitting methods described in the text. (b) The deduced step heights at the surface, defined as the difference between every two adjacent points in (a).

by 1 AL. The error bars indicate the spread in values from the different fitting methods. These values show clear quasibilayer oscillations, particularly for the smaller thicknesses. For larger thicknesses, the error bars get progressively wider, commensurate with the increase in film roughness as shown in Figs. 5 and 6.

It should be noted that the term "step height" as used here refers to the vertical distances between the terrace heights of two thicknesses differing by 1 AL. The local step height encountered by an atom diffusing across the surface of the sample may be different, since additional lattice distortions in the regions very near to the step edges probably occur to minimize the local strain and shear energies. That is, the diagram in Fig. 1 is not indicative of the local region around a step edge, but rather a schematic showing how the atomic layers in the (terraces of) different regions of thickness may be misaligned. Furthermore, lateral Friedel oscillations originating from the step edges have been observed in the electron density,[47,48] which can also affect the lattice structure. However, such edge effects will be limited to a relatively local region (within a few lattice spacings) near the step edges. Since HAS is a scattering technique, it measures the statistical average of the scattering from the atomic planes, and STM studies generally measure the heights of atomic terraces over an extended range. Thus, edge effects can be neglected in such comparisons.

The oscillations in Fig. 10(b) are consistent with the STM results of Ref. 27, where it should be noted that the N values differ from ours by 1 AL because we include the wetting layer in N. However, the amplitude of the oscillations in Fig. 10 is much smaller than that in Fig. 4(b) of Ref. 27, which may be partly attributable to the fact that STM measures the electron density at the surface, which may not reflect the true positions of the atomic cores. Similarly, our results are also consistent with those found in the HAS study of Ref. 26.

V. SUMMARY

We have presented surface x-ray-diffraction results of the growth and layer structure (strain) of Pb/Si(111) films with thicknesses of 6–19 AL. At 110 K the system is found to follow a metastable layer-by-layer growth mode with increasing roughness. The extended x-ray-reflectivity profiles were found to have distinctive half-order features present that are indicative of a quasibilayer periodicity to the lattice structure. To describe the lattice distortions in the context of QSE, a free-electron model is derived that takes into account the formation of quantum well states in the film and describes the Friedel-like oscillations in the electronic charge density of the film. The free-electron model is found to explain the quasibilayer lattice distortions of the film and enable a detailed fit of the experimental data.

Extended x-ray-reflectivity profiles at integer coverages were obtained and analyzed to reveal the thickness dependence of the structural properties of the film. Quasibilayer oscillations are also observed in the outermost lattice relaxations as a function of thickness, similar to oscillations seen in other physical properties of the films due to QSE. Finally, the deviations from the ideal film thicknesses are deduced and compared to previous STM and HAS studies, where the present results are found to qualitatively agree, albeit with a smaller amplitude of oscillation. It can be concluded that quantum confinement has important effects on the physical structure of a nanoscale film.

ACKNOWLEDGMENTS

We thank Mei-Yin Chou and Ching-Ming Wei for helpful discussions. This work is based on work supported by the U.S. Department of Energy, Division of Materials Sciences (Grant No. DEFG02-91ER45439). The UNICAT facility at the Advanced Photon Source (APS) is supported by the U.S. Department of Energy through the Frederick Seitz Materials Research Laboratory at the University of Illinois at Urbana-Champaign, the Oak Ridge National Laboratory, the National Institute of Standards and Technology, and UOP LLC. The APS is supported by the U.S. Department of Energy (Grant No. W-31-109-ENG-38). We also acknowledge partial equipment and personnel support from the Petroleum Research Fund, administered by the American Chemical Society, and the U.S. National Science Foundation (Grant No. DMR-02-03003).

*Electronic address: chiang@mrl.uiuc.edu

[1] F. K. Schulte, Surf. Sci. **55**, 427 (1976).
[2] J. M. Blatt and C. J. Thompson, Phys. Rev. Lett. **10**, 332 (1963).
[3] B. G. Orr, H. M. Jaeger, and A. M. Goldman, Phys. Rev. Lett. **53**, 2046 (1984).
[4] Y. Guo Y.-F. Zhang, X.-Y. Bao, T.-Z. Han, Z. Tang, L.-X. Zhang, W.-G. Zhu, E. G. Wang, Q. Niu, Z. Q. Qiu, J.-F. Jia, Z.-X. Zhao, and Q.-K. Xue, Science **306**, 1915 (2004).
[5] T.-C. Chiang, Science **306**, 1900 (2004).
[6] M. Valden, X. Lai, and D. W. Goodman, Science **281**, 1647 (1998).
[7] D.-A. Luh, T. Miller, J. J. Paggel, and T.-C. Chiang, Phys. Rev. Lett. **88**, 256802 (2002).
[8] N. D. Lang and W. Kohn, Phys. Rev. B **1**, 4555 (1970).
[9] Z. Zhang, Q. Niu, and C.-K. Shih, Phys. Rev. Lett. **80**, 5381 (1998).
[10] S. Ciraci and I. P. Batra, Phys. Rev. B **33**, 4294 (1986).
[11] T. Valla, M. Kralj, A. Šiber, M. Milun, P. Pervan, P. D. Johnson, and D. P. Woodruff, J. Phys.: Condens. Matter **12**, L477 (2000).
[12] T.-C. Chiang, Surf. Sci. Rep. **39**, 181 (2000).
[13] L. Aballe, A. Barinov, A. Locatelli, S. Heun, and M. Kiskinova, Phys. Rev. Lett. **93**, 196103 (2004).
[14] P. J. Feibelman, Phys. Rev. B **27**, 1991 (1983).
[15] L. Gavioli, K. R. Kimberlin, M. C. Tringides, J. F. Wendelken, and Z. Zhang, Phys. Rev. Lett. **82**, 129 (1999).
[16] K. Budde, E. Abram, V. Yeh, and M. C. Tringides, Phys. Rev. B **61**, R10602 (2000).
[17] G. Materzanini, P. Saalfrank, and P. J. D. Lindan, Phys. Rev. B **63**, 235405 (2001).
[18] D.-A. Luh, T. Miller, J. J. Paggel, M. Y. Chou, and T.-C. Chiang, Science **292**, 1131 (2001).
[19] R. Otero, A. L. Vázquez de Parga, and R. Miranda, Phys. Rev. B **66**, 115401 (2002).
[20] A. Mans, J. H. Dil, A. R. H. F. Ettema, and H. H. Weitering, Phys. Rev. B **66**, 195410 (2002).
[21] C. M. Wei and M. Y. Chou, Phys. Rev. B **66**, 233408 (2002).
[22] P. Czoschke, H. Hong, L. Basile, and T.-C. Chiang, Phys. Rev. Lett. **91**, 226801 (2003).
[23] H. Hong, C.-M. Wei, M. Y. Chou, Z. Wu, L. Basile, H. Chen, M. Holt, and T.-C. Chiang, Phys. Rev. Lett. **90**, 076104 (2003).
[24] P. Czoschke, H. Hong, L. Basile, and T.-C. Chiang, Phys. Rev. Lett. **93**, 036103 (2004).
[25] A. Crottini, D. Cvetko, L. Floreano, R. Gotter, A. Morgante, and F. Tommasini, Phys. Rev. Lett. **79**, 1527 (1997).
[26] J. Braun and J. P. Toennies, Surf. Sci. **384**, L858 (1997).
[27] W. B. Su, S. H. Chang, W. B. Jian, C. S. Chang, L. J. Chen, and T. T. Tsong, Phys. Rev. Lett. **86**, 5116 (2001).
[28] M. Hupalo, S. Kremmer, V. Yeh, L. Berbil-Bautista, E. Abram, and M. C. Tringides, Surf. Sci. **493**, 526 (2001).
[29] M. Hupalo, V. Yeh, L. Berbil-Bautista, S. Kremmer, E. Abram, and M. C. Tringides, Phys. Rev. B **64**, 155307 (2001).
[30] M. Hupalo and M. C. Tringides, Phys. Rev. B **65**, 115406 (2002).
[31] V. Yeh, L. Berbil-Bautista, C. Z. Wang, K. M. Ho, and M. C. Tringides, Phys. Rev. Lett. **85**, 5158 (2000).
[32] U. Landman, R. N. Hill, and M. Mostoller, Phys. Rev. B **21**, 448 (1980).
[33] J.-H. Cho, Ismail , Z. Zhang, and E. W. Plummer, Phys. Rev. B **59**, 1677 (1999).
[34] J. A. Carlisle, T. Miller, and T.-C. Chiang, Phys. Rev. B **45**, 3400 (1992).
[35] P. B. Howes, K. A. Edwards, D. J. Hughes, J. E. Macdonald, T. Hibma, T. Bootsma, and M. A. James, Phys. Rev. B **51**, 17740 (1995).
[36] P. B. Howes, K. A. Edwards, D. J. Hughes, J. E. Macdonald, T. Hibma, and M. A. James, Surf. Sci. **331–333**, 646 (1995).
[37] P. B. Howes, K. A. Edwards, J. E. Macdonald, T. Hibma, T. Bootsma, M. A. James, and C. L. Nicklin, Surf. Rev. Lett. **5**, 163 (1998).
[38] M. H. Upton, C. M. Wei, M. Y. Chou, T. Miller, and T.-C. Chiang, Phys. Rev. Lett. **93**, 026802 (2004).
[39] M. H. Upton, T. Miller, and T.-C. Chiang, Appl. Phys. Lett. **85**, 1235 (2004).
[40] I. K. Robinson and D. J. Tweet, Rep. Prog. Phys. **55**, 599 (1992).
[41] I. K. Robinson and E. Vlieg, Surf. Sci. **261**, 123 (1992).
[42] J. Als-Nielsen and D. McMorrow, *Elements of Modern X-Ray Physics* (Wiley, Chichester, 2001).
[43] E. D. Specht and F. J. Walker, J. Appl. Crystallogr. **26**, 166 (1993).
[44] K. A. Edwards, P. B. Howes, J. E. Macdonald, T. Hibma, T. Bootsma, and M. A. James, Surf. Sci. **424**, 169 (1999).
[45] Y. S. Li, F. Jona, and P. M. Marcus, Phys. Rev. B **43**, 6337 (1991).
[46] C. M. Wei and M. Y. Chou (unpublished).
[47] A. Samsavar, E. S. Hirschorn, T. Miller, F. M. Leibsle, J. A. Eades, and T.-C. Chiang, Phys. Rev. Lett. **65**, 1607 (1990).
[48] M. F. Crommie, C. P. Lutz, and D. M. Eigler, Nature (London) **363**, 524 (1993).